Colloids and Surfaces B: Biointerfaces 164 (2018) 144–154

Contents lists available at ScienceDirect

Colloids and Surfaces B: Biointerfaces

journal homepage: www.elsevier.com/locate/colsurfb

Self-sterilizing ormosils surfaces based on photo-synzthesized silver nanoparticles

Lidiane Patrícia Gonçalves[a], Alejandro Miñán[b], Guillermo Benítez[b], Mónica Fernández Lorenzo de Mele[b], María Elena Vela[b], Patricia L. Schilardi[b], Elias Paiva Ferreira-Neto[a], Júlia Cristina Noveletto[a], Wagner Rafael Correr[c], Ubirajara Pereira Rodrigues-Filho[a,*]

[a] Grupo de Química de Materiais Híbridos e Inorgânicos, Prédio de Química Ambiental, Instituto de Química de São Carlos, Universidade de São Paulo, 13563-120, São Carlos, SP, Brazil

[b] Instituto de Investigaciones Fisicoquímicas Teóricas y Aplicadas (INIFTA), Facultad de Ciencias Exactas, UNLP – CONICET, CC 16 Suc 4(1900) La Plata, Argentina

[c] Centro de Tecnologia de Materiais Híbridos, Grupo Crescimento de Cristais e Materiais Cerâmicos, Instituto de Física de São Carlos e Escola de Engenharia de São Carlos, Universidade de São Paulo, 13563-120, São Carlos, SP, Brazil

ARTICLE INFO

Article history:
Received 24 July 2017
Received in revised form
20 November 2017
Accepted 10 December 2017
Available online 26 December 2017

Keywords:
Antibacterial activity
Pseudomonas aeruginosa
Staphylococcus aureus
Ormosil
Ag nanoparticles

ABSTRACT

Medical device-related infections represent a major healthcare complication, resulting in potential risks for the patient. Antimicrobial materials comprise an attractive strategy against bacterial colonization and biofilm proliferation. However, in most cases these materials are only bacteriostatic or bactericidal, and consequently they must be used in combination with other antimicrobials in order to reach the eradication condition (no viable microorganisms). In this study, a straightforward and robust antibacterial coating based on Phosphotungstate Ormosil doped with core-shell (SiO_2@TiO_2) was developed using sol-gel process, chemical tempering, and Ag nanoparticle photoassisted synthesis (POrs-CS-Ag). The coating was characterized by X-ray Fluorescence Spectroscopy (XRF), Field Emission Scanning Electron Microscopy (FE-SEM), Atomic Force Microscopy (AFM) and X-ray Photoelectron Microscopy (XPS). The silver free coating displays low antibacterial activity against *Staphylococcus aureus* and *Pseudomonas aeruginosa*, in opposition to the silver loaded ones, which are able to completely eradicate these strains. Moreover, the antimicrobial activity of these substrates remains high until three reutilization cycles, which make them a promising strategy to develop self-sterilizing materials, such as POrs-CS-Ag-impregnated fabric, POrs-CS-Ag coated indwelling metals and polymers, among other materials.

1. Introduction

Mitigation of hospital-acquired infections has become a great concern due to the increasing bacterial resistance to conventional antibiotics [1]. It has encouraged the development of new antimicrobial materials and coatings based in innovative biocidal strategies able to control bacterial attachment and proliferation [2–4]. In this sense, some interesting approaches are: a) modification of surfaces either by physical patterns (micropatterned surfaces) [5–7] or by surface functionalization with antimicrobial molecules to reduce the rate of bacterial colonization [8]; b) polymer coatings that control the release of antimicrobial agents (antibiotics, silver ions or nanoparticles), and/or mixed polymers with self-cleaning and self-sterilization properties [9]; c) inorganic coatings with intrinsic antimicrobial activity such as titanium dioxide, a well-known photosensitizer upon UV light irradiation that provides a high rate of bacterial inactivation [10]. Nevertheless, these promising strategies have some limitations. Reduction of bacterial colonization by chemical or physical methods does not imply sterilization, and re-growth of microorganisms may occur. In case of drug release from a polymer matrix, antimicrobial load is limited and the release kinetics may determine the antimicrobial

Abbreviations: Ormosil, organically modified silicate; CS, core@shell; NPs, nanoparticles; AgNPs, silver nanoparticles; POrs, phosphotungstate ormosils; POrs-CS, phosphotungstate ormosils doped with core@shell; POrs-Ag, phosphotungstate ormosils doped with silver; POrs-CS-Ag, phosphotungstate ormosil doped with core@shell and silver.

* Corresponding author. Present address: Grupo de Quimica de Materiais Hibridos e Inorganicos, Instituto de Quimica de São Carlos, Universidade de São Paulo, 13563-120, São Carlos, São Paulo, Brazil.
E-mail address: ubirajara@usp.br (U.P. Rodrigues-Filho).

https://doi.org/10.1016/j.colsurfb.2017.12.016
0927-7765/

concentration over time [11]. On the other hand, photodynamic inactivation of microorganisms by TiO_2 is achieved by UV exposure, which can only be done before the implantation. Thus, bacterial proliferation can occur if the indwelling device is contaminated during surgical procedures. Considering these points, the development of new antimicrobial materials with prolonged bactericidal activity and able to attain the sterilization of surfaces is essential in order to significantly reduce the morbidity and mortality risks of implantation procedures.

In the last years, sol-gel processing emerged as a versatile methodology for coating surfaces with multifunctional purposes [12–16] that include several bio-applications such as enzyme [17,18], living cells [19] and fungi entrapment for biocatalysis [20]. Although the capacity of the sol-gel process to produce versatile coatings able to enhance the interaction between biomaterials and living cells is well known, only few efforts have been made to exploit the use of this procedure to obtain antibacterial coatings. Among them, Yin et al. have reported an active antibacterial coating based on mixed Layer-by-Layer method and sol-gel process [21] for multifunctional coating deposition on a cellulose substrate, while Tay et al. developed antimicrobial silsesquioxane–silica hybrids by hydrolytic co-condensation of alkoxysilanes [22]. Recently Gong et al. reported the effect of AH Plus, a commercial antimicrobial product, incorporated to quaternary ammonium epoxy silicate against *Enterococcus faecalis*, resulting in a promising approach for controlling endodontic infection 23. In our group we have exploited the use of phosphotungstic acid as a catalyst to obtain flat xerogels films and coatings [16,24,25]. The use of this superacid [26] allows efficient catalysis of the hydrolysis co-condensation reactions to obtain the sol used for coating preparation. Phosphotungstate Keggin clusters are excellent photocatalysts [27], especially after adsorption on wide band semiconductors such as TiO_2 [28].This photocatalytical enhancement is based on photoelectron transfer from the semiconductor to the LUMO of the phosphotungstate yielding heteropolyblues formation [24]. Titania entrapment in the phosphotungstate ormosils (organically modified silicates) resulted in increase on photochromic response of the ormosils, as previously reported by our group [29]. Thus, this enhanced photocatalytic behavior would be used for the formation of silver nanoparticles through the entrapment of Ag(I) ions and the subsequent photoreduction of these ions.

Although the use of TiO_2 nanoparticles (NPs) is attractive, they tend to aggregate inside the films, thus resulting in lower surface area and lower activity [24].This agglomeration can be overcome by using TiO_2NPs dispersed on silica sub-micron particles [30]. Cation loaded xerogels can be useful for the preparation of multifunctional materials, including antibacterial ones. A very straightforward methodology for cation incorporation on xerogel films is the chemical tempering. Chemical tempering is a glass hardening technique based on ion-exchange in molten salts [31]. Such approach for cation metal absorption induces a cation gradient in the films with metal cation enrichment on the ormosil surface. Phosphotungstate in ormosil coating can act as a cation exchange site, exchanging protons by Ag^+ and forming $H_{3-x}Ag_x[PW_{12}O_{40}]$ species [32]. The noble metal phosphotungstate formed is a precursor for synthesis of noble metal/phosphotungstate heterostructures. In fact, polyoxometalate/TiO_2 heterojunction was first used by Pearson et al. [28] to produce Au nanoparticles decorated phosphotungstate@TiO_2 particles while Mandal et al. [33] achieved the photoreduction of silver cations by polyoxometalates.

The antibacterial silver NPs phosphotungstate heterostructures $H_{3-x}Ag_x[PW_{12}O_{40}]$ can be achieved by electron transfer from reduced phosphotungstate to the silver cations. These reduced phosphotungstates can be formed by thermal or photochemical reduction. The phosphotungstate/TiO_2 heterojunction increase the yield of photogenerated heteropolyblues which, in turn, can conduct to a high yield in the AgNPs formation. Furthermore, these phosphotungstate/TiO_2 heterojunctions can spatially drive the NPs distribution on the surface and inside the supporting material. So far, the photoassisted formation of AgNPs by Keggin polyoxoanion inside supporting materials has not been previously explored. Thus, this procedure could be innovatively applied to prepare AgNPs loaded materials. Improvement on reduction of silver cations by photoreduced polyoxometalate can be obtained by using TiO_2 dispersed on silica sub-micron particles due to the higher surface area presented by these core@shell particles [30]. AgNPs loaded materials have attracted large interest in the literature and from several industries around the Globe, because of the above mentioned antibacterial properties [34–36], among many other outstanding properties.

We report here a reproducible and easily prepared coating with antibacterial activity based on hybrid Phosphotungstate ormosils (POrs hereafter) loaded with AgNPs. These AgNPs were photosynthesized by UV irradiation of the phosphotungstate/SiO_2@TiO_2 heterojunction entrapped in the ormosil coating. Two are the main novelties in the present manuscript. First, to the best of our knowledge, the preparation of the silver nanoparticle by chemical tempering followed by irradiation promoting such well dispersed and high loaded AgNP at/on the surface with good control of particle size distribution based on UV–vis spectrum has not yet been reported. This combined processing is versatile and can be easily scaled up. Detailed surface and physicochemical characterization of the novel silver-loaded coatings is presented, as well as microbiological assays using *Pseudomonas aeruginosa* (*P. aeruginosa*) and *Staphylococcus aureus* (*S. aureus*) in order to evaluate their antimicrobial and self-sterilizing properties. Importantly, only a tiny amount of SiO_2@TiO_2 is necessary to achieve the antibacterial effects and self-sterilization (total eradication of viable bacteria), which is attained due to the action of AgNPs-loaded surfaces even without further irradiation. Notice that very few systems are capable to eradicate bacteria, being active up to three bacteria exposition cycles. Thus, the material developed in this work is unique, since its ability for killing bacteria, reaching total eradication, is better than other previously reported in the literature. In fact, to our best knowledge antibacterial surfaces previously developed are able to inhibit the bacterial growth and proliferation, without achieving self-sterilization. The bacteria eradication efficiency is certainly related to the AgNP formation and loading protocol based on the unique combination of chemical tempering and nanoparticle photoassisted formation by photoreduced phosphotungstate.

2. Experimental section

2.1. Materials

Tetraethylorthosilicate (TEOS 98%), *3-Glycidoxypropiltrimetoxysilane* (GLYMO, 98%), 4-(triethoxysilyl)butyronitrile (BuTS, 98%), hydrated phosphotungstic acid (reagent grade), and $AgNO_3$ (ACS reagent, Vetec) were purchased from Sigma-Aldrich (USA) and were used without further purification. Ethanol (99.8%) was supplied by Quemis (SP, Brazil) and ultrapure water was obtained from a Marconi Water Purification unit (water resistivity, 18MΩ).Soda-lime glass slides were purchased from Bioslide (Bioslide Technologies, Canada).

2.2. Synthesis of core-shell NPs

The SiO_2@TiO_2 core-shell NPs, referred as CS from now on, were prepared according to Ullah et al. [30]. Briefly, SiO_2 particles (previously prepared by Stöber method [37] were dried at 110 °C for at least 1 h 0.2 g of the dried silica powder was dispersed in 40 mL iso-

propanol by sonication for 1 h. The suspension and additional 50 mL of isopropanol were transferred to a closed Teflon reactor. Subsequently, 220 uL of titanium tetraisopropoxide was added and the mixture was kept under magnetic stirring for 20 h. Hydrolysis of the titanium alkoxide precursor was then promoted by dropwise addition of 3 mL water/6 mL isopropanol solution. After 1 h kept under magnetic stirring, the suspension was centrifuged for 10 min at 3500 rpm, washed once with isopropanol and re-suspended in 35 mL of deionized water. The aqueous suspension was then transferred to a homemade Teflon lined brass hydrothermal reactor and submitted to hydrothermal treatment at 105 °C for 24 h. Finally, the CS particles were obtained by centrifugation of the suspension, washed twice with deionized water and dried at 80 °C for 24 h

2.3. Preparation of the phosphotungstate ormosils doped with CS

The procedure for preparation of the hybrid films was adapted from Ferreira-Neto et al. [15]. Roughly, TEOS (9 mmol) and BuTS (1.5 mmol) were dissolved in 25 mL of anydrous ethanol under magnetic stirring. A second solution was prepared by dissolving 0.75 mmol of hydrated phosphotungstic acid (HPW) in 25 mL of ethanol and added to the alkoxysilane solution. After the mixed solution was kept under stirring for 5 min, 45 mmol of deionized water and 6.8 mmol of GLYMO were slowly added. Finally, different volumes of ethanolic CS particles suspension were added according to Table T1 (Suppl. Inf.). The obtained sol was stirred for additional 10 min before being used for film preparation by dip coating.

2.4. Substrate cleaning and film preparation

The films, containing POrs and POrs doped with CS (POrs-CS),were prepared following the protocol reported by Gonçalves et al., 29. Firstly, soda-lime glass slides were cleaned using a cleaning solution ($NH_4OH/H_2O_2/H_2O$ in 1:1:5 vol ratio) at 70 °C for 2 h. Then, the glass substrates (25 mm^2) were washed with deionized water and dried under a steam of nitrogen.

Finally, the films were prepared using the Marconi Dip-coating equipment (Marconi, Brazil). For each sample, the clean glass substrate was subjected to 20 immersions to obtain the multilayer films. The immersion and emersion velocity was set to 150 mm/min.

2.5. Chemical tempering with Ag^+

The silver cation loading process was adapted from traditional chemical tempering technique [31], i.e. ionic exchange by immersing the POrs films in 1 M $AgNO_3$ aqueous solution at room temperature. To find the higher loading conditions, an ion exchange kinetic experiment using a silver nitrate solution, was performed. Once determined the tempering time for higher loading, the silver loading was carried out and the substrate was dried under air at room temperature in dark conditions for 24 h.

2.6. Photoassisted synthesis of AgNPs

The photoassisted formation of the AgNPs in the different hybrid films was studied by UV–vis electronic absorption spectroscopy after exposure to UV radiation using a Solar Light Simulator with a Xe arc lamp (model 16S–150 W, fabricated by Solar Light Company, Inc., Philadelphia, USA). The spot size diameter at the sample was 1 cm, the sample to UV source exit was set to 7.3 cm, and the maximum irradiance was 750 W m^{-2}. For microbiological testing, AgNPs formation in the hybrid films was carried out using a pencil style Oriel 6035 Hg lamp positioned at a 10 cm distance from the sample in order to completely expose the samples to UV radiation. Irradiation time was set for 10 min since further irradiation did not show significant increase in the films absorbance employing such irradiation conditions. Following this procedure, AgNPs were formed in ormosil (POrs and POrs-CS) substrates, which were denoted as POrs-Ag and POrs-CS-Ag.

2.7. Material characterization

2.7.1. XPS

All spectra were collected using a non-monochromatic Al Kα x-ray source (XR50, SPECS GmbH), a hemispherical electron analyzer (Phoibos 100, SPECS GmbH). The survey spectra were collected using a pass energy of 40 eV, while high resolution spectra were recorded using 10 eV. All samples were POrs and POrs-CS films on glass substrate with and without AgNPs. The charging correction was performed using the C peak at 285 eV as internal reference. Spectra fitting was performed with XPS Peak 4.1 software, using a Shirley type background and a product of Gaussian and Lorentzian functions for the peaks.

2.7.2. Electronic (UV–vis) spectroscopy

All spectra of the films were collected using a Shimadzu UV-3600 spectrophotometer in transmission mode with the hybrid films supported on soda-lime glass slides perpendicular to the radiation beam.

2.7.3. X-ray fluorescence

Elemental analysis of Ag present in the films was performed using a benchtop X-ray fluorescence spectrometer Minipal 4 (Panalytical, Netherlands) with a Rh X-ray tube, power set to 9W, acquisition time 500s, under helium atmosphere. The analyzed films were deposited on SiO_2/Si(100) wafers, previously cleaned with piranha solution. The silver quantifications were made by standardless techniques based on fundamental parameters [38].

2.7.4. Field emission scanning electron microscopy (FE-SEM)

The FEG-SEM images were obtained in an Inspect F50 (FEI, The Netherlands). The beam accelerating voltage was set to 30 kV to get deeper beam penetration, allowing imaging the CS particles several nanometers underneath the film surface. Images were formed using backscattered electrons (BSE) signal which provides chemical contrast (Z contrast). Energy Dispersive Spectroscopy (EDS) was performed in a line scan mode over CS particles to determine the location of silver and titanium using an Apollo X SDD detector (EDAX, USA) and a beam acceleration of 15 kV.

2.7.5. Atomic force microscopy (AFM)

AFM images were obtained with a Multimode microscope controlled by a Nanoscope V control unit (Bruker, USA), in Tapping® mode. The tips used were RTESPA (Bruker,spring constant, k = 20–80 N m^{-1}; oscillating resonance frequency 370 – 310 kHz). All images were analyzed using the Nanoscope Analysis 7.2 software.

2.8. Antimicrobial assays

2.8.1. Bacterial culture

S. aureus (ATCC 25923) and *P. aeruginosa* (clinical isolate) were chosen as models of Gram (+) and Gram (−) opportunistic pathogens, respectively. Strains were grown overnight in nutrient broth (NB; Merck, Darmstadt, Germany) at 28 °C in a rotary shaker (250 rpm). Each bacterial inoculum was diluted in NB in order to get ~10^8 colony-forming units (CFU) mL^{-1} of bacteria for viability assays. The CFU values were confirmed by plate counting method.

2.8.2. Sessile bacteria assay

Bacterial adhesion assays were performed as described by Flores et al. [35] with minor modifications. Briefly, bacterial suspensions were adjusted to ~10^8 CFU mL^{-1} in fresh NB and used immediately for the inoculation of the substrates. Glass substrates were used as control. The substrates were vertically placed in the bacterial suspension and incubated at 28 °C for 2 h. After that, the substrates were removed and gently washed by immersing them in double-distilled sterile water in order to discard cells that were not tightly attached to the surface.

The enumeration of viable sessile bacteria on the substrates was performed by plate counting method: the substrates were individually placed in glass tubes containing 2 mL of sterile PBS and the irreversibly adherent bacteria were detached by sonication for 15 min using a Testlab sonicator (40 Khz with power output of 160 W). Then, the quantification of bacteria in the suspension was estimated by plating appropriate dilutions on nutrient agar (Britania, Argentina). The experiments were made thrice and the plating was carried out in duplicate. No effect of sonication on the number of surviving cell was found [34]. Statistical analysis was performed using one-way analysis of variance (ANOVA) to evaluate differences between groups of bacteria. A p value <0.05 was considered statistically significant.

2.8.3. Antimicrobial properties of reused silver loaded substrates

The antimicrobial activity of reused silver loaded substrates (POrs-Ag and POrs-CS-Ag) was determined by growing halo assays. To this end, bacterial adhesion on the POrs-CS-Ag and POrs-Ag coated surfaces was carried out as described in 2.8.2. Then, the substrates were washed in double-distilled sterile water and placed in sterile nutrient agar plates at 28 °C for 24 h. After this period, bacterial growth around the POrs-Ag and POrs-CS-Ag was examined. To evaluate if POrs-CS-Ag maintains its antibacterial properties after reuse, in each assay the substrate was removed and washed in double-distilled sterile water and the procedure (2 h-bacterial adhesion and further nutrient agar plate incubation) was repeated with each substrate until bacterial colonies were visualized. The absence of colonies around or under the substrate indicates that the antimicrobial activity is conserved in the silver loaded substrate.

3. Results and discussion

3.1. Characterization of silver loaded substrates

3.1.1. Chemical tempering

The time dependence of the Ag^+ loading in the POrs-CS films was followed by X-Ray Fluorescence of the Ag inside the films and the results are shown in Fig. S1 (Suppl. Inf.) for the CS100 one as a representative curve for the complete set of ormosils tested. Silver cation loading steeply increases during the first minutes of immersion and a fast saturation is reached after 10 min. The fast absorption profile is typical of ion-exchange sorption since no covalent bond needs to be broken during ion-exchange, therefore this mechanism would explain the silver cation loading observed in POrs-CS and POrs films.

It is important to stress that chemical tempering does follow the Fickís second law. Therefore, a concentration gradient along the film thickness in the ormosil samples is built up. Such gradient, as expected from the Fickís second law, will proportionate a higher silver concentration on the outermost layers of the film. Such asymmetric concentration profile will be advantageous for the antibacterial activity since the higher silver concentration in the outermost layers will release enough silver ions into culture media to attain the bactericidal effect.

3.1.2. Photoassisted synthesis of AgNPs

Photo-assisted reduction of Ag^+ to form AgNPs by phosphotungstate adsorbed on TiO_2 and photoreduced $=TiO_2//H[PW_{12}O_{40}]^{3-}$ should follow the Eqs. (1)–(3):

$$= TiO_{2//}[PW_{12}O_{40}]^{3-} + h\nu \rightarrow = TiO_{2//}[[PW_{12}O_{40}]^{3-}{}_{excited} \quad (1)$$

$$= TiO_{2//}[[PW_{12}O_{40}]^{3-}{}_{excited} + HX_{reduced} \rightarrow = TiO_{2//}[H[PW_{12}O_{40}]^{3-} + X_{oxidized} \quad (2)$$

$$n = TiO_{2//}[H[PW_{12}O_{40}]^{3-} + nAg^{+} \rightarrow n = TiO_{2//}[H[PW_{12}O_{40}]^{2-} + Ag_n{}^{0}{}_{(s)} \quad (3)$$

Where HX stands for a proton donor such as ethanol or water absorbed during the film formation process.

Formation of AgNPs in the UV irradiated films was studied by UV–vis electronic absorption spectroscopy by monitoring appearance of AgNPs characteristic surface plasmon resonance (SPR) absorption band. The electronic absorption spectra of the hybrid films after UV exposure are shown in Fig. 1. The SPR absorption wavelength and peak area values for the different samples are summarized in Table T2 (Suppl. Inf.).

Ag^+ loaded POrs and POrs-CS absorption spectra exhibited the typical AgNPs plasmonic band at maximum absorption wavelengths (λ_{max}) in the range of 400–411 nm [39], whose absorbance increases as the time of UV exposure does (Fig. 1a), reflecting an increasing photoconversion of Ag^+ into AgNPs. The relatively narrow and symmetric line shapes of the plasmonic absorption are qualitative indicators of narrow size distribution of the particles and their high dispersion in the hybrid films, since the band widening expected for NPs agglomeration is not observed [40].

Plasmon absorption frequency (ϖ_M) depends of both the electrical permittivity due to the electrons ($\varepsilon_1{}^d$) and the contribution from the surrounding media (ε_m), consequently, plasmonic band wavelength is determined not only by particle electrical permittivity but also by the surrounding medium, as given by the Eq. (4) below [41]

$$\omega_M = \frac{\omega_P}{\sqrt{\left[\varepsilon_1{}^d(\omega_M) + 2\varepsilon_m\right]}} \quad (4)$$

For noble metal NPs it is necessary to take into account the electron spill over correction, which includes the size dependence of the frequency, according to Eq. (5) [40].·, where ϖ_p stands for bulk plasmon frequency, $\varpi_M(R_{Ne})$ stands for the size dependent corrected plasmon frequency, R_{Ne} stands for the particle radius and δ is an adjustable parameter.

$$\omega_{M(R_{Ne})} \approx \omega_{M^{classic}} \left(1 - \frac{3\delta}{2R_{Ne}}\right) \quad (5)$$

The centroid of the plasmonic band at 400–411 nm is indicative of average crystal sizes in the range of 15–30 nm for the photosynthesized AgNPs [42]. Since no significant changes were observed either in the plasmon absorption λ_{max} or in band width for the POrs-CS-Ag film as a function of irradiation time (Fig. 1a), a very fast nucleation rate for the process is expected, in agreement with photoreduction electron transfer mechanism, which may be promoted by both CS particles and the photoreduced polyoxometalate species. In fact, the presence of CS particles was shown to increase formation of AgNPs, as indicated by the larger plasmonic band area values for the CS-doped films as compared to the undoped sample

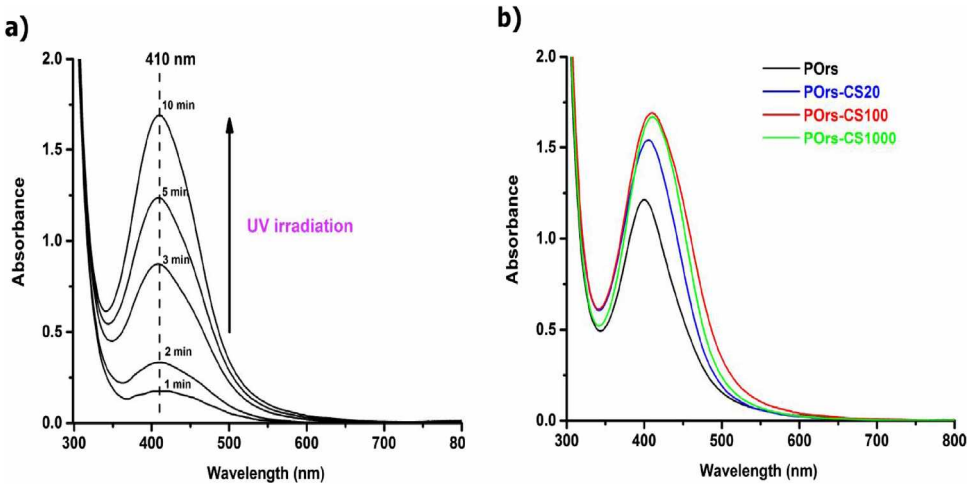

Fig. 1. UV–vis electronic extinction spectra of sample Ag^+-POrs-CS100 after various UV irradiation intervals (a); Comparison of the electronic spectra of CS-doped and undoped Ag^+-POrs hybrid films after 10 min of UV irradiation (b).

(Table T2, Suppl. Inf.), a maximum increase of 62% been observed for sample POrs-CS100. Additionally, CS-doped films SPR bands also displayed slightly red-shifted λ_{max} values, which indicate a change in the surrounding dielectric medium or larger size of AgNPs. The SiO_2@TiO_2 CS particles may enhance photo-induced formation of AgNPs by both promoting direct photocatalytic reduction of Ag^+ cations [43] and by increasing formation of photoreduced phosphotungstate species [28,39], which may also promote formation of AgNPs [44]. In this way, both photocatalysts, CS particles and phosphotungstate polyoxoanions, act synergistically for the photo-assisted formation of AgNPs in the hybrid ormosil films.

3.1.3. Field emission scanning electron microscopy (FE-SEM)

The formation of AgNPs around the CS inside the POrs-CS100 was studied by Field Emission Scanning Electron Microscopy (FE-SEM) of the POrs films on glass slides using field gun tension at 30 kV. Under this condition is possible to probe the underneath layer of the POrs, thus observing the buried CS particles. To improve the contrast, the backscattered electron detector (BSE) was used. The backscattered electron detector (BSE) signal shows brighter regions due to the domains with higher mean atomic number. Accordingly, the formation of a silver or TiO_2 deposit on the submicron SiO_2 particles can be noticed in the image shown in Fig. 2. In order to chemically characterize these submicron particles, the EDS line scan data was collected over two CS particles (white line in Fig. 2). The silicon X-ray emission signal is slightly higher on the submicron particles region (red line), as expected. Furthermore, the shell formation is evidenced by a sudden increase in silver and titanium signal counts at the particles edges (dashed lines). Thus, the results reinforce the hypothesis stated in Eqs. (1)–(3), since the presence of the core@shell@shell(SiO_2@TiO_2//$H[PW_{12}O_{40}]^{2-}$ nanostructure was observed in FE-SEM images.

3.1.4. Atomic force microscopy

The surface morphology and roughness of the POrs with silver cation (non-irradiated) before and after irradiation were studied by ex-situ AFM tapping mode. We have employed the root mean square roughness (RMS) Rq (Eq. (6)) to evaluate the roughness of the surfaces which is the standard deviation of the Z values within a given area, as described in Eq. (6).

$$R_q = \sqrt{\frac{\sum_{i=1}^{N}(Z_i - Z_{ave})^2}{N}} \quad (6)$$

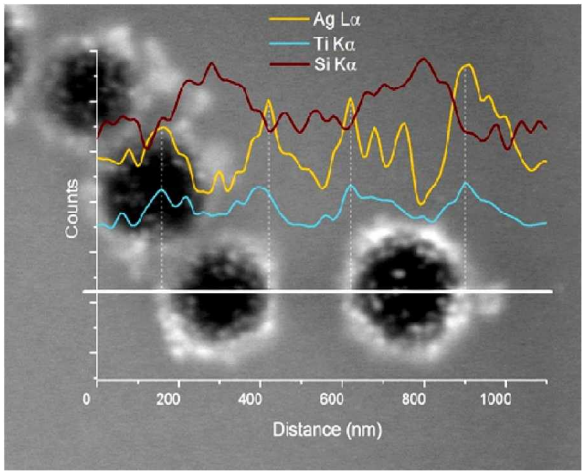

Fig. 2. Field emission Scanning Electron Microscopy of the CS-Ag particle (i.e. Ag@SiO2@TiO2) in the POrs-CS100-Agfilm. Superposed to the image it is the X-ray emission intensity for the Ag Lα and Ti Kαlines along the white line. The abscissa in the inserted graph shows the distance along the line in nm, while the ordinate shows the X-ray emission intensity.

Where Z_i is the value of z at a point i of the surface, Z_{ave} is the average value within the given area and N is the number of points within that area [45,46].

The effect of irradiation on the morphology of CS was evaluated by cross section analysis. After irradiation, the topography is similar for all samples (Fig. 3). However, the average size of the particles is higher than those values found for the samples before irradiation.

The values of Rq measured on 10 μm × 10 μm images of the samples with and without silver are shown in Table T3 (Suppl. Inf.).

These data show a decrease in surface roughness for all substrates after irradiation, although this effect is not proportionally scaled with the amount of CS. UV annealing of the sol-gel films, including Ormosils, has been previously reported for laser UV excimers as well as Hg arc lamp [47–49] being related to dehydroxylation and condensation reactions for vacuum UV sources or organic moieties degradation in the UV A/B region. The Si—O bond is highly stable toward thermal and photoactivated cleavage, however, the photochemical cleavage can be achieved by deep UV if Si—H or Si—C are present, thus suffering homolytic cleavage and forming reactive radicals [50]. The Xe arc lamp used in this work has longer wavelength cut-off than the previously reported source and far less power density, therefore, it would be unlikely

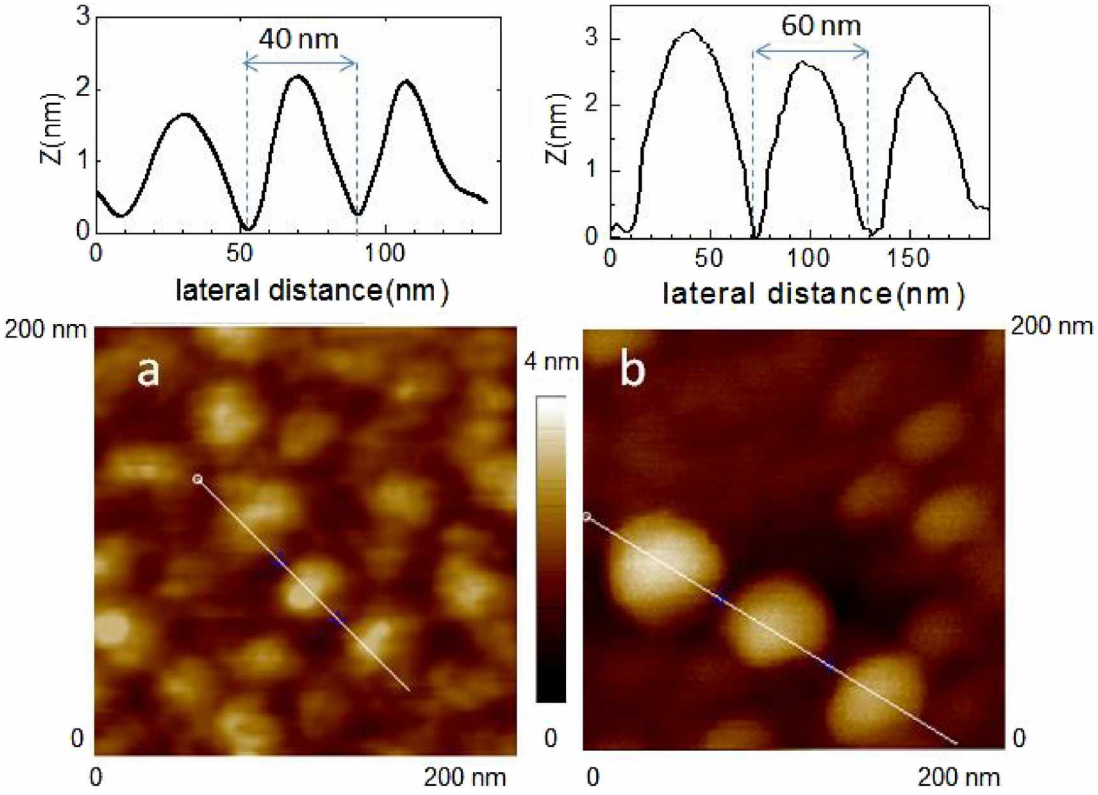

Fig. 3. Cross section analysis of representative images of Ormosil surfaces modified with silver (a) before (b) after irradiation. The z-color scale is the same for both images.

any silanol or siloxane bond breaking in the ormosils without CS, thus the observed surface changes can be related to UV annealing or photodegradation of the surface organic functionalities. The surface flattening effect is more pronounced for the Ormosil with larger content of CS. Therefore, this effect must be related to the UV-induced photocatalytic activity of these CS particles which promotes higher organics degradation due to generation of hydroxyl radicals. On the other hand, it should be considered an alternative interpretation: silver would be deposited in a conformal way following the core-shell structure. The decrease in roughness could be attributed to the filling of the valleys between particles. Both interpretations would require a model in order to assess the structure of the compounds on the surface, which is out of scope of the present work.

3.1.5. X-ray photoemission spectroscopy (XPS)

The maximum depth of analysis for XPS is around 10 nm depending on the film density, take-off angle and X-ray energy [51]. XPS can retrieve the average composition of the POrs surfaces [15,52] thus helping to the understanding of surface phenomena such as bacterial adhesion and bactericide effect.

The survey scan for the silver loaded samples before and after irradiation shows the expected photoelectric and Auger lines for the O1s, W4f doublet, C1s, N1s, Ag 3d and Si 2p (Fig. S2, Suppl. Inf.). Therefore, it is possible to infer the presence of phosphotungstate and silver on the outmost layer of the ormosils, which is relevant for the antibacterial properties. An interesting remark is the presence of asymmetric $W4f_{7/2}$ and $W4f_{5/2}$ spin-orbit doublets. The asymmetric doublets were fitted to two pseudo-Voigt doublets with $W4f_{7/2}$ at 35 eV and 36.1 eV (Fig. S3, Suppl. Inf.). The 35 eV component was tentatively assigned to highly dispersed phosphotungstate interacting with surrounding media by comparison with previous studies by XPS [13]. Binding energies of polyoxoanions are very susceptible to the matrix environment due to intermolecular interactions with organic surface moieties [53]. So, XPS measurements confirm the presence of phosphotungstate in two different environments, one clearly related to the phosphotungstic acid species and the other was tentatively assigned to the SiO_2@TiO_2//$H[PW_{12}O_{40}]^{2-}$.

The high-resolution XP-Ag 3d region for the non-irradiated (NI) silver cation loaded or irradiated (I) ones POrs films, with and without CS particles are shown in Fig. 4. The spectra show the typical spin-orbit splitting for the $Ag3d_{5/2}$ and $Ag3d_{3/2}$ doublet. The binding energies for the $Ag3d_{5/2}$ span between 368 and 369 eV typical values for Ag^+ and Ag^0 [54–58]. Furthermore differential charging can complicate the assignment of the oxidation state of silver in hybrid films [59] as well as particle size distribution [60]. Nevertheless, the most important feature remains clear, that is the presence of silver species on the surface of the ormosils.

3.1.6. Silver release study

As it has been previously discussed, the effect of Ag-NPs may be directly related to the NPs or to the silver ions that are released from their surface [35]. In order to evaluate the stability and possible release of silver in culture media, quantification of the total silver content (cationic and NPs) of POrs films before and after immersion (2 h) in the culture media was followed by X-ray fluorescence spectroscopy (XRF) (Fig. S4, Suppl. Inf.). Results reveal that in all cases the amount of silver content of the films tested decreases after immersion in the culture media, which can be assigned to both, silver ions and/or Ag NPs released to the liquid medium.

3.2. Evaluation of antimicrobial properties of silver loaded substrates

3.2.1. Viability of bacteria adhered to ormosils substrates

3.2.1.1. Bacterial adhesion on ormosils substrates without AgNPs. In this study, opportunistic clinical pathogen, *S. aureus* and *P.*

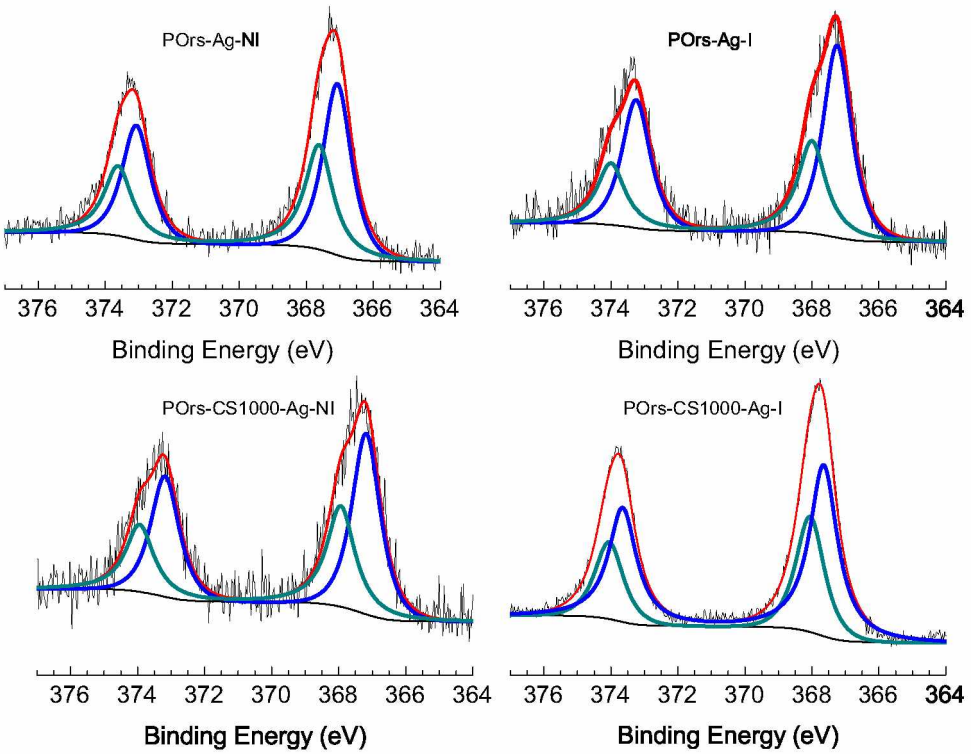

Fig. 4. High resolution XP-Ag 3d region for the silver cation loaded on non-irradiated (NI) and irradiated (I) POrs films with and without CS particles. The spectra show the typical spin-orbit splitting for the $Ag3d_{5/2}$ and $Ag3d_{3/2}$ doublet.

aeruginosa, were chosen as models of Gram positive and Gram negative microorganisms, respectively. Substrates were immersed in bacterial culture and the enumeration of *P. aeruginosa* and *S. aureus* cells attached to ormosil films and glass substrates were carried out (Fig. 5). The number of viable sessile cells of *P. aeruginosa* attached to POrs and POrs-CS is similar to that found on the control substrate ($p > 0.05$). Thus, these results reveal that *Pseudomonas* showed no selectivity for the adhesion on ormosil substrates without AgNPs (POrs, POrs-CS20, POrs-CS100, POrs-CS1000, Fig. 5A). Besides, bacterial adhesion was similar for all the assayed substrates regardless the presence or absence of CS particles. It has been previously reported that the formation of *Pseudomonas* aggregates on the substrate immersed in abiotic culture media is not dependent on the physical-chemical properties of its surface [61]. The non-selective adhesion of *Pseudomonas* to the surfaces can be partially explained by the coverage of the surfaces by adsorbed organic species coming from the culture medium forming a conditioning layer suitable for the attachment of several microorganisms [61] and by the extracellular polymeric substances (EPS) that partially masks surface properties.

On the other hand, the adhesion of *S. aureus* cells on POrs films decreased at least 5-fold compared with the control ($p < 0.05$) (Fig. 5B). The adhesion of *S. aureus* is influenced by the composition of the surface. Thus, a lower adherence was found for CS-containing substrates. Conversely, *P. aeruginosa*, known by their ubiquity and high production of EPS were not affected by the characteristics of the substrate.

3.2.1.2. Ormosils films loaded with AgNPs. When the antimicrobial activity of ormosils films loaded with AgNPs was analyzed, a dramatic decrease in the viability of bacteria was observed (Fig. 5). Remarkably, no viable sessile cells of *P. aeruginosa* or *S. aureus* were found on POrs-Ag and POrs-CS-Ag which emphasized the strong eradicating activity of these substrates that leads to self-sterilization. It should be noted that the high bactericidal effect of silver loaded ormosil films was reached even in the case of POrs-Ag which does not contain CS particles and presented a slightly lower formation of AgNPs.

Although *P. aeruginosa* showed an exceptional ability to colonize non-loaded metal ormosil substrates, the incorporation of AgNPs into the film decreased dramatically its viability attaining self-sterilization. Much effort has been devoted to the development of biomaterials with effective antimicrobial properties for medical devices in order to prevent biofilms-related infection. Recently Pappas et al. [9] developed an innovative mixed polymeric surface to inactivate bacterial pathogens. Even though this polymeric material shows promising application as an antimicrobial surface, it was not able to reach the total killing of the attached bacteria (20–30% of the initial inoculum remained viable). In fact, this mixed polymeric film exhibited a good bacteriostatic activity but was not able to attain a complete sterilization of the surface. Similarly, several approaches based on AgNPs-coated surfaces resulted in good bacteriostatic activity persisting in time [35,62–64]. At this point is worth to stress that antibacterial surfaces are defined as those able to inhibit the growth and proliferation of microorganisms [65] and, therefore, it is expected that they only complement the conventional antibiotic treatment. However, in clinical practice, bactericidal activity is required in order to avoid biofilm-related infections associated to indwelling devices. On this regard, the important step forward made by silver loaded ormosil substrates presented in this work is the total eradication of bacteria attached to the surface, without the requirement of UV irradiation, i.e. even in darkness, which is also a significant advantage compared with those materials based in irradiated TiO_2 coatings that need irradiation and are not able to eradicate bacteria.

Even though the antimicrobial properties of Ag, either as ions or NPs, against a wide variety of microorganisms (bacteria, fungal and virus) are well known, the mechanism involved in the antimicrobial properties of AgNPs is controversial and remains unclear. The most accepted mechanisms include (i) the release of Ag(I) which interact

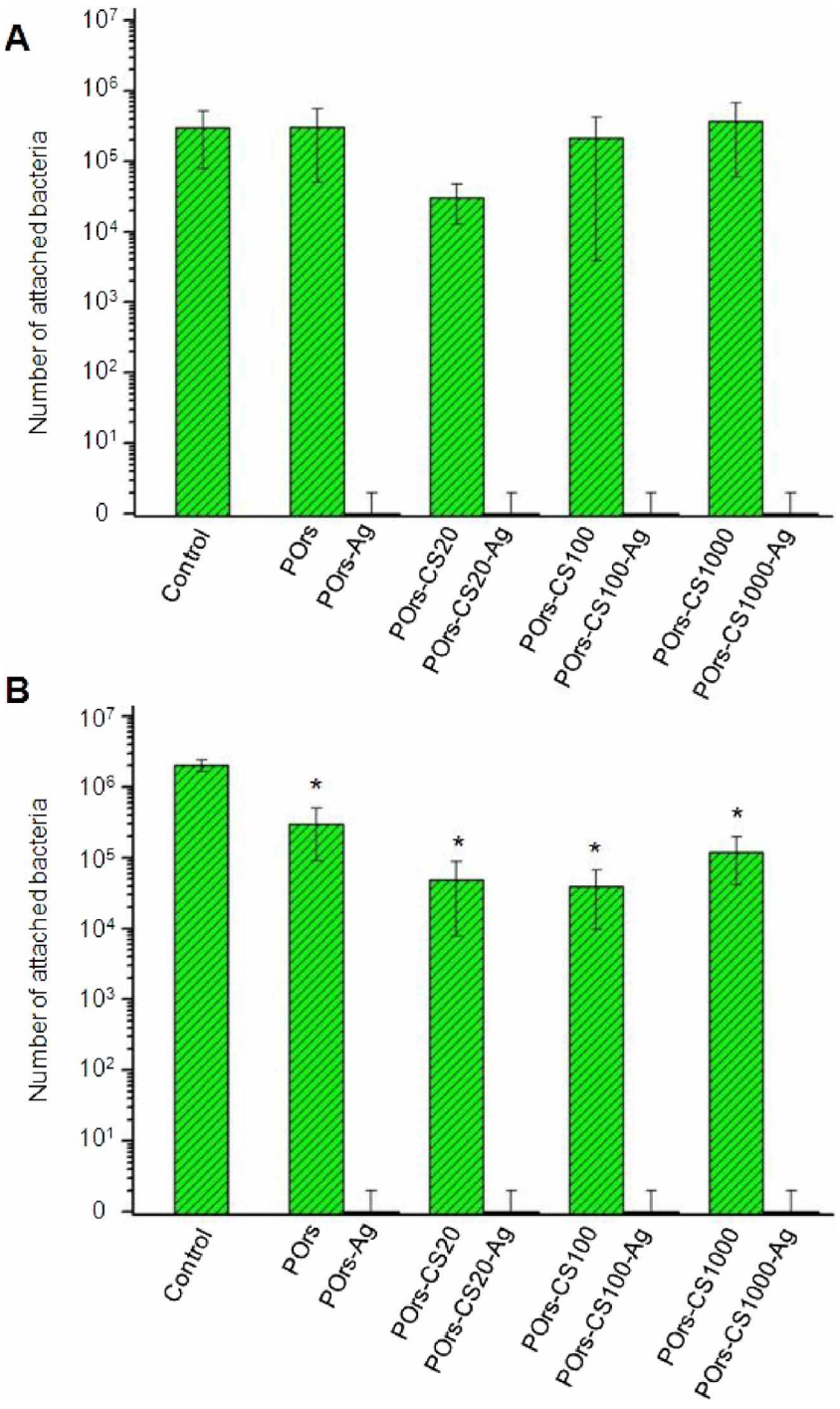

Fig. 5. Bacterial colonization on ormosil substrates. Enumeration of *P. aeruginosa* (A) and *S. aureus* (B) viable sessile cells on different ormosil substrates with and without AgNPs. Glass surface was used as control. In all cases Ag-containing substrates showed complete eradication of bacteria since no viable bacteria was found (red bars). * indicates significant difference ($p < 0.05$) between control and ormosil substrates (glass slides of 25 mm^2). (For interpretation of the references to colour in this figure legend, the reader is referred to the web version of this article.)

with thiol groups in proteins (ii) the internalization of AgNPs, which may inhibit DNA replication, block bacterial respiration chain, and may generate ROS [66] and (iii) the inhibition of the enzymatic activity by AgNPs, promoting cell wall disruption. Based on the XRF analysis (Fig. S4, Suppl. Inf.) it was demonstrated that silver release is occurring into the culture media. However, both silver cation and AgNPs display high antibacterial activity, and therefore their individual action is out of scope of this work. As regards our experimental results involving POrs-Ag and POrs-CS-Ag surfaces, although the silver release is different for these substrates (Fig. S4), all of them are able to reach bacterial eradication (Fig. 5). It seems that the silver release from all the assayed substrates is higher than a threshold value able to eradicate bacteria and no difference in the efficacy is found. Thus, it is reasonable to speculate that the killing mechanism is linked to the action of a threshold value of silver ions concentration.

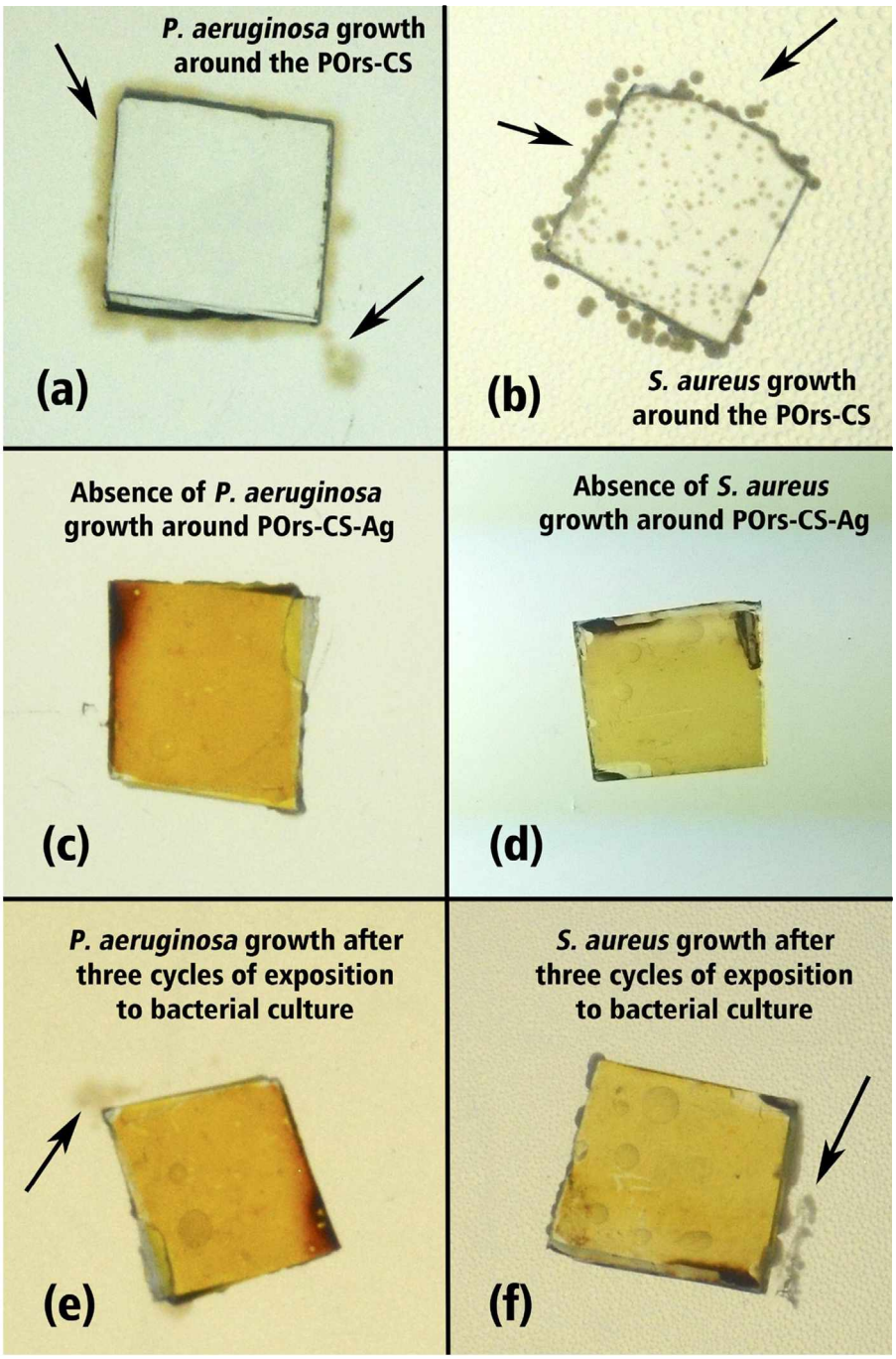

Fig. 6. Growing halo assays showing the effectiveness of self-sterilization of POrs-CS-Ag due to Ag incorporation after the first exposition to bacterial cultures: bacterial growth on POrs-CS, (a) and (b); Absence of bacterial growth on POrs-CS-Ag (bacterial eradication), (c) and (d). Similar results were obtained after the second immersion of the POrs-CS-Ag in the bacterial culture. Weak bacterial proliferation around the POrs-CS-Ag substrates after three reusing cycles, (e) and (f), as denoted by the arrows.

3.2.2. Bacterial growth around POrs-CS and POrs-CS-Ag surfaces. Effect of reutilization on antibacterial properties

The possibility of re-utilization of POrs-CS-Ag coated materials was analyzed. After the immersion of the sample in the bacterial culture medium and placing it on the agar surface, bacteria attached on the POrs-CS were able to grow on the agar (Fig. 6a and b). However, when the same procedure was repeated with POrs-CS-Ag no bacteria grew on the agar, indicating the effectiveness of the self-sterilizing POrs-CS-Ag surface (Figs. 6c and d).

To evaluate if the POrs-CS-Ag surfaces were able to retain the antibacterial activity, they were tested after being immersed two and three times in the bacterial culture, that is, the substrates were exposed to the most extreme conditions. No bacterial growth was observed after the first and second cycle (Figs. 6c and d), and only a weak cell proliferation was found after the third cycle (Figs. 6e and f). From these results, it is reasonable to infer that the silver loaded POrs-CS films exposed to air or a less aggressive aqueous environment than agar surface will be able to retain the antimicrobial activity for longer periods of time (higher than 3 cycles), a fact that reinforces the idea that these substrates are promising self-sterilizing surfaces. An additional advantage of these materials is the successful adhesion of ormosils on indwelling materials without harmful effects on vascular cells [67], which increases the scope of the approach reported in this study.

4. Conclusions

Chemical Tempering followed by photoassisted silver nanoparticle synthesis inside sol-gel prepared POrs and POrs-CS films is a versatile and reproducible methodology for preparing self-sterilizing films able to adhere on indwelling materials without harmful effects on vascular cells. Moreover, these films are easily applied on glass substrate using a simple scale-up processing. Results demonstrated that silver loaded ormosil substrates are able to achieve eradication (no viable bacteria on the surface) of nosocomial pathogens such as *P. aeruginosa* and *S. aureus*, Importantly, the antimicrobial activity of these substrates remains at least until three reutilization cycles under a very aggressive condition. In summary, the biocidal properties of this coating, able to achieve self-sterilization without needing irradiation, together with the reutilization of these POrs-CS-Ag coated substrates makes this coating, to the best of our knowledge, as one of best strategies to avoid bacterial adhesion on surfaces.

Funding

Fundação de Amparo à Pesquisa do Estado de São Paulo (FAPESP) and Conselho Nacional de Desenvolvimento Científico e Tecnológico (CNPq). Universidad Nacional de La Plata and ANPCyT.

Acknowledgments

The Brazilian authors thanks to Fundação de Amparo à Pesquisa do Estado de São Paulo (FAPESP) grants #2013/50619-7 and 2011/08120-0. L.P. Gonçalves thanks Conselho Nacional de Desenvolvimento Científico e Tecnológico (CNPq) for a studentship in Brazil and Coordenação de Aperfeiçoamento de Pessoal de Nível Superior (CAPES) for an internship at La Plata, Argentina, for nine months during her PhD. The Argentinian authors are grateful to CONICET, UNLP (grants 11/X665 and 11/X760) and ANPCyT (PICT 2010-1779 and PICT 2012-1795). MEV is member of the research career of CIC PBA.

Appendix A. Supplementary data

Supplementary data associated with this article can be found, in the online version, at https://doi.org/10.1016/j.colsurfb.2017.12.016.

References

[1] Antimicrobial Resistance Global Report on Surveillance, Fact Sheet N°194 Updated April 2015, World Health Organization, 2014.
[2] Q. Yu, J. Cho, P. Shivapooja, L.K. Ista, G.P. López, Nanopatterned smart polymer surfaces for controlled attachment: killing, and release of bacteria, ACS Appl. Mater. Interfaces 5 (19) (2013) 9295–9304.
[3] X. Dai, Z. Fan, Y. Lu, P.C. Ray, Multifunctional nanoplatforms for targeted multidrug-resistant-bacteria theranostic applications, ACS Appl. Mater. Interfaces 5 (21) (2013) 11348–11354.
[4] L. Wang, U.J. Erasquin, M. Zhao, L. Ren, M.Y. Zhang, G.J. Cheng, Y. Wang, C. Cai, Stability, antimicrobial activity and cytotoxicity of poly (amidoamine) dendrimers on titanium substrates, ACS Appl. Mater. Interfaces (2011) 2885–2894.
[5] C. Diaz, P.L. Schilardi, R.C. Salvarezza, M.F. de Mele, Nano/microscale order affects the early stages of biofilm formation on metal surfaces, Langmuir 23 (22) (2007) 11206–11210.
[6] C. Diaz, A. Minan, P. Schilardi, L. Fernandez, M. Lorenzo de Mele, Synergistic antimicrobial effect against early biofilm formation: micropatterned surface plus antibiotic treatment, Int. J. Antimicrob. Agents 40 (3) (2012) 221–226.
[7] A. Miñán, P. Schilardi, M. Fernández Lorenzo, Antimicrobial resistance of Staphylococcus aureus: importance of 2D aggregates on the subsequent resistance of biofilms, Biofoul. Manuscr. (2012), ID GBIF-2012-0312 Enviado.
[8] J. Grischke, J. Eberhard, M. Stiesch, Antimicrobial dental implant functionalization strategies—a systematic review, Dent. Mater. J. 35 (4) (2016) 545–558.
[9] H.C. Pappas, S. Phan, S. Yoon, L.E. Edens, X. Meng, K.S. Schanze, D.G. Whitten, D.J. Keller, Sterilizing self-cleaning mixed polymeric multifunctional antimicrobial surfaces, ACS Appl. Mater. Interfaces 7 (50) (2015) 27632–27638.
[10] L. Visai, L. de Nardo, C. Punta, L. Melone, A. Cigada, M. Imbriani, C.R. Arciola, Titanium oxide antibacterial surfaces in biomedical devices, Int. J. Artif. Organs (2011) pp 929–946.
[11] M.C. Cortizo, T.G. Oberti, M.S. Cortizo, A.M. Cortizo, M.A.F.L. de Mele, Chlorhexidine delivery system from titanium/polybenzyl acrylate coating: evaluation of cytotoxicity and early bacterial adhesion, J. Dent. 40 (4) (2012) 329–337.
[12] R. Pardo, M. Zayat, D. Levy, Photochromic organic–inorganic hybrid materials, Chem. Soc. Rev. 40 (2011) 672–687.
[13] C. Sanchez, B. Lebeau, F. Chaput, J.-P. Boilot, Optical properties of functional hybrid organic-inorganic nanocomposites, Adv. Mater. 15 (23) (2003) 1969.
[14] J.C. Carls, P. Argitis, A. Heller, Deep ultraviolet photoresist based on tungsten polyoxometalates and poly(vinyl alcohol) for bilayer photolithography, J. Electrochem. Soc. 139 (3) (1992) 786–793.
[15] E. Ferreira-Neto, F.L.S. P.; De Carvalho, S. Ullah, V.C. Zoldan, A. Pasa, A.L. A.; De Souza, L.C. Battirola, P. Rudolf, S.A. Bilmes, U.P. Rodrigues-Filho, Surface structure and reactivity study of phosphotungstic acid-nitrogenated ormosils, J. Sol-Gel Sci. Technol. 66 (3) (2013) 363–371.
[16] E.P. Ferreira-Neto, S. Ullah, F.L.S. De Carvalho, A.L. De Souza, M. De Oliveira, J.F. Schneider, Y.P. Mascarenhas, A.M. Jorge, U.P. Rodrigues-Filho, Preparation, characterization and photochromic behavior of phosphotungstic acid-ormosil nanocomposites, Mater. Chem. Phys. 153 (2015) 410–421.
[17] L.F.F.F. Gonçalves, F.K. Kanodarwala, J.A. Stride, C.J.R. Silva, M.J.M. Gomes, One-pot synthesis of CdS nanoparticles exhibiting quantum size effect prepared within a sol-gel derived ureasilicate matrix, Opt. Mater. (Amst) 36 (2) (2013) 186–190.
[18] H. Frenkel-Mullerad, R. Ben-Knaz, D. Avnir, Preserving the activity of enzymes under harsh oxidizing conditions: sol-gel entrapped alkaline phosphatase exposed to bromine, J. Sol-Gel Sci. Technol. 69 (2) (2014) 453–456.
[19] S. Chia, J. Urano, F. Tamanoi, B. Dunn, J.I. Zink, Patterned hexagonal arrays of living cells in sol-gel silica films [1], J. Am. Chem. Soc. 122 (27) (2000) 6488–6489.
[20] L.C. Rocha, A. De Souza, U.P. Rodrigues, S.P. Campana Filho, L.D. Sette, A.L.M. Porto, Immobilization of marine fungi on silica gel, silica xerogel and chitosan for biocatalytic reduction of ketones, J. Mol. Catal. B Enzym. 84 (2012) 160–165.
[21] Y. Yin, C. Wang, Y. Wang, Fabrication and characterization of self-assembled multifunctional coating deposition on a cellulose substrate, Colloids Surf. A Physicochem. Eng. 399 (2012) 92–99.
[22] S.-Q.S. Gong, D.J. Epasinghe, W. Zhang, B. Zhou, L.-N.L. Niu, H. Ryou, A.A. Eid, A. Frassetto, C.K.Y. Yiu, D.D. Arola, J. Mao, D.H. Pashley, F.R. Tay, Synthesis of antimicrobial Silsesquioxane–silica hybrids by hydrolytic co-condensation of alkoxysilanes, Polym. Chem. 5 (2) (2014) 454.
[23] S.Q. Gong, Z. Huang, W. Bin Shi, B. Ma, F.R. Tay, B. Zhou, In vitro evaluation of antibacterial effect of AH plus incorporated with quaternary ammonium epoxy silicate against Enterococcus faecalis, J. Endod. 40 (10) (2014) 1611–1615.
[24] S. Ullah, J.J.S. Acuña, A.A. Pasa, S.A. Bilmes, M.E. Vela, G. Benitez, U.P. Rodrigues-Filho, Photoactive layer-by-layer films of cellulose phosphate and titanium dioxide containing phosphotungstic acid, Appl. Surf. Sci. 277 (2013) 111–120.
[25] E.P. Ferreira-Neto, S. Ullah, O.A.E. Ysnaga, U.P. Rodrigues-Filho, Zn^{2+} doped ormosil-phosphotungstate hybrid films with enhanced photochromic response, J. Sol-Gel Sci. Technol. 72 (2) (2014) 290–300.
[26] R.S. Drago, J.A. Dias, T.O. Maier, An acidity scale for bronsted acids including $H_3PW_{12}O_{40}$, J. Am. Chem. Soc. 119 (33) (1997) 7702–7710.
[27] Y. Guo, C. Hu, Heterogeneous photocatalysis by solid polyoxometalates, J. Mol. Catal. A Chem. 262 (1–2) (2007) 136–148.
[28] R.R. Ozer, J.L. Ferry, Investigation of the photocatalytic activity of TiO_2 – polyoxometalate systems, Environ. Sci. Technol. 35 (15) (2001) 3242–3246.
[29] L.P. Gonçalves, E.P. Ferreira-Neto, S. Ullah, L.V. de Souza, O.A.E. Ysnaga, M.V. dos Santos, S.J.L. Ribeiro, U.P. Rodrigues-Filho, Enhanced photochromic response of ormosil-phosphotungstate nanocomposite coatings doped with TiO_2 nanoparticles, J. Sol-Gel Sci. Technol. 76 (2) (2015) 386–394.
[30] S. Ullah, E.P. Ferreira-Neto, A. a. Pasa, C.C.J. Alcântara, J.J.S. Acuña, S. a. Bilmes, M.L. Martínez Ricci, R. Landers, T.Z. Fermino, U.P. Rodrigues-Filho, Enhanced photocatalytic properties of core@shell SiO_2@TiO_2 nanoparticles, Appl. Catal. B Environ. 179 (2015) 333–343.
[31] R. Gy, Ion exchange for glass strengthening, Mater. Sci. Eng. B Solid-State Mater. Adv. Technol. 149 (2) (2008) 159–165.
[32] W. Liang, C. Huang, L. Ma, Controllable synthesis of polyoxometalates nanocubes and their specific interactions with prion proteins, Sci. China Ser. B Chem. 52 (12) (2009) 2156–2160.
[33] S. Mandal, D. Rautaray, M. Sastry, Ag^+-Keggin ion colloidal particles as novel templates for the growth of silver nanoparticle assemblies, J. Mater. Chem. 13 (12) (2003) 3002.
[34] K. Vasilev, V.R. Sah, R.V. Goreham, C. Ndi, R.D. Short, H.J. Griesser, Antibacterial surfaces by adsorptive binding of polyvinyl-sulphonate-stabilized silver nanoparticles, Nanotechnology 21 (21) (2010) 215102.
[35] C.Y. Flores, A.G. Miñán, C.A. Grillo, R.C. Salvarezza, C. Vericat, P.L. Schilardi, Citrate-capped silver nanoparticles showing good bactericidal effect against both planktonic and sessile bacteria and a low cytotoxicity to osteoblastic cells, ACS Appl. Mater. Interfaces 5 (8) (2013) 3149–3159.

[36] P. Pallavicini, A. Taglietti, G. Dacarro, Y. Antonio Diaz-Fernandez, M. Galli, P. Grisoli, M. Patrini, G. Santucci De Magistris, R. Zanoni, Self-assembled monolayers of silver nanoparticles firmly grafted on glass surfaces: low Ag^+ release for an efficient antibacterial activity, J. Colloid Interface Sci. 350 (1) (2010) 110–116.
[37] W.E.R.N.E.R. Stober, Controlled growth of monodisperse silica spheres in the micron size range, J. Colloid Interface Sci. 69 (1968) 62–69.
[38] V.A. Solé, E. Papillon, M. Cotte, P. Walter, J. Susini, A multiplatform code for the analysis of energy-dispersive X-ray fluorescence spectra, Spectrochim. Acta – Part B At. Spectrosc. 62 (1) (2007) 63–68.
[39] R.A. Ganeev, M. Baba, A.I. Ryasnyansky, M. Suzuki, H. Kuroda, Characterization of optical and nonlinear optical properties of silver nanoparticles prepared by laser ablation in various liquids, Opt. Commun. 240 (4–6) (2004) 437–448.
[40] A. Perez, P. Mélion, J. Lermé, P.-F. Brevet, Clusters and colloids, in: C. Dupas, P. Houdy, M. Lahmani (Eds.), Nanoscience: Nanotechnologies and Nanophysics, 2004, pp. 179–279.
[41] H. Horvath, Gustav mie and the scattering and absorption of light by particles: historic developments and basics, J. Quant. Spectrosc. Radiat. Trans. 110 (11) (2009) 787–799.
[42] S. Agnihotri, S. Mukherji, S. Mukherji, Size-controlled silver nanoparticles synthesized over the range 5–100 nm using the same protocol and their antibacterial efficacy, RSC Adv. 4 (8) (2014) 3974–3983.
[43] K. Naoi, Y. Ohko, T. Tatsuma, TiO_2 films loaded with silver nanoparticles: control of multicolor photochromic behavior, J. Am. Chem. Soc. 126 (11) (2004) 3664–3668.
[44] W. Qi, H. Li, L. Wu, Stable photochromism and controllable reduction properties of surfactant-encapsulated polyoxometalate/silica hybrid films, J. Phys. Chem. B 112 (28) (2008) 8257–8263.
[45] I. Metrology, Userís and Reference Guide. Version 4.4, 1st ed., Image Metrology, Copenhagen, 1998.
[46] A. Méndez-Vilas, J.M. Bruque, M.L. González-Martín, Sensitivity of surface roughness parameters to changes in the density of scanning points in multi-scale AFM studies. Application to a biomaterial surface, Ultramicroscopy 107 (8) (2007) 617–625.
[47] P. Innocenzi, G. Brusatin, A comparative FTIR study of thermal and photo-polymerization processes in hybrid sol-gel films, J. Non. Cryst. Solids 333 (2) (2004) 137–142.
[48] R.E. Van De Leest, M.J.A. Horikx, P.W.H. Hermans, Photodesorption studies on thin film sol-gel systems, Appl. Surf. Sci. 106 (1996) 412–417.
[49] X.Y. Zhang, W. Chen, Z.M. Wang, J.Y. Zhang, I.W. Boyd, UV annealing of inorganic-organic composite films prepared by sol-gel technique, Thin Solid Films 453 (454) (2004) 59–62.
[50] J. Pola, A. Galíková, A. Galík, V. Blechta, Z. Bastl, J. Šubrt, A. Ouchi, UV laser photolysis of disiloxanes for chemical vapor deposition of nano-textured silicones, Chem. Mater. 14 (1) (2002) 144–153.
[51] J.F. Watts, J. Wolstenholme, Comparison of XPS and AES with other analytical techniques, in: An Introduction to Surface Analysis by XPS and AES, John Wiley & Sons, Ltd., 2003, pp. 165–182.
[52] D. Sprenger, H. Bach, W. Meisel, P. Gütlich, Discrete bond model (DBM) of sodium silicate glasses derived from XPS: Raman and NMR measurements, J. Non. Cryst. Solids 159 (3) (1993) 187–203.
[53] F.C. De Oliveira, J. Schneider, A. Siervo, R. Landers, A.M.G. Plepis, J.J. Pireaux, U.P. Rodrigues-Filho, Micro – and nanocomposites of Keggin heteropolymetalates in cellulose esters, Surf. Interface Anal. 34 (1) (2002) 580–582.
[54] U.P. Rodrigues-Filho, Y. Gushikem, M. Do Carmo Gonçalves, R.C. Cachichi, S.C. De Castro, Composite membranes of cellulose acetate and zirconium dioxide: preparation and study of physicochemical characteristics, Chem. Mater. 8 (7) (1996) 1375–1379.
[55] P. Bazant, I. Kuritka, L. Munster, L. Kalina, Microwave solvothermal decoration of the cellulose surface by nanostructured hybrid Ag/ZnO particles: a joint XPS, XRD and SEM study, Cellulose 22 (2) (2015) 1275–1293.
[56] N. Feng, Q. Wang, A. Zheng, Z. Zhang, J. Fan, S.-B. Liu, J.-P. Amoureux, F. Deng, Understanding the high photocatalytic activity of (B, Ag) – codoped TiO_2 under solar-light irradiation with XPS, solid-state NMR and DFT calculations, J. Am. Chem. Soc. 135 (2013) 1607–1616.
[57] S.F. Ho, S. Contarini, J.W. Rabalais, Ion-beam-induced chemical changes in the oxyanions (moyn-) and oxides (mox) where M = chromium: molybdenum, tungsten, vanadium, niobium and tantalum, J. Phys. Chem. 91 (18) (1987) 4779–4788.
[58] W. Grunert, R. Schlogl, H.G. Karge, Investigations of zeolites by photoelectron and ion-scattering spectroscopy. 1. New applications of surface spectroscopic methods to zeolites by a high-temperature measurement technique, J. Phys. Chem. 97 (33) (1993) 8638–8645.
[59] L.J. Gerenser, Photoemission investigation of silver/poly (ethylene terephthalate) interfacial chemistry: the effect of oxygenplasma treatment photoemission investigation of silver/poly (ethylene terephthalate) interfacial chemistry, Effect Oxygen-Plasm 2011 (3682) (1990).
[60] M. Taner-Camcı, S. Suzer, Dynamic XPS measurements of ultrathin polyelectrolyte films containing antibacterial Ag–Cu nanoparticles, J. Vac. Sci. Technol. A Vac. Surf. Film 32 (2) (2014) 21510.
[61] C. Diaz, R.C. Salvarezza, M.F.L. Mele, P.L. de Schilardi, Organization of pseudomonas fluorescens on chemically different nano/microstructured surfaces, ACS Appl. Mater. Interfaces 2 (9) (2010) 2530–2539.
[62] M.A. Massa, C. Covarrubias, M. Bittner, I.A. Fuentevilla, P. Capetillo, A. Von Marttens, J.C. Carvajal, Synthesis of new antibacterial composite coating for titanium based on highly ordered nanoporous silica and silver nanoparticles, Mater. Sci. Eng. C 45 (2014) 146–153.
[63] Y.K. Jo, J.H. Seo, B.H. Choi, B.J. Kim, H.H. Shin, B.H. Hwang, H.J. Cha, Surface-independent antibacterial coating using silver nanoparticle-generating engineered mussel glue, ACS Appl. Mater. Interfaces 6 (22) (2014) 20242–20253.
[64] Z. Li, D. Lee, X. Sheng, R.E. Cohen, M.F. Rubner, Two-level antibacterial coating with both release-killing and contact-killing capabilities, Langmuir 22 (24) (2006) 9820–9823.
[65] E. Ivanova, R. Crawford (Eds.), Antibacterial Surfaces, Springer International Publishing, Cham, 2015.
[66] S. Agnihotri, S. Mukherji, S. Mukherji, Immobilized silver nanoparticles enhance contact killing and show highest efficacy: elucidation of the mechanism of bactericidal action of silver, Nanoscale 5 (16) (2013) 7328–7340.
[67] F.G. Doro, A.P. Ramos, J.F. Schneider, M.A.M.S. Veiga, C.L. Yano, A. Negreti, M.H. Krieger, E. Tfouni, Deposition of organic – inorganic hybrid coatings over 316 L surgical stainless steel and evaluation on vascular cells, Can. J. Chem. 995 (2014) 987–995.